NANO LETTERS
Letter
Cite This: Nano Lett. 2019, 19, 5489−5495
pubs.acs.org/NanoLett

Elongated Lifetime and Enhanced Flux of Hot Electrons on a Perovskite Plasmonic Nanodiode

Yujin Park,[†,‡] Jungkweon Choi,[†,‡,§] Changhwan Lee,[‡,∥] An-Na Cho,[⊥] Dae Won Cho,[#] Nam-Gyu Park,[⊥] Hyotcherl Ihee,[*,†,‡,§] and Jeong Young Park[*,†,‡,∥]

[†]Department of Chemistry, Korea Advanced Institute of Science and Technology (KAIST), Daejeon 305-701, Republic of Korea
[‡]Center for Nanomaterials and Chemical Reactions, Institute for Basic Science (IBS), Daejeon 305-701, Republic of Korea
[§]KI for the BioCentury, Korea Advanced Institute of Science and Technology (KAIST), Daejeon 305-701, Republic of Korea
[∥]Graduate School of EEWS, Korea Advanced Institute of Science and Technology (KAIST), Daejeon 305-701, Republic of Korea
[⊥]School of Chemical Engineering and Department of Energy Science, Sungkyunkwan University, Suwon 440-746, Republic of Korea
[#]Department of Advanced Materials Chemistry, Korea University, Sejong Campus, Sejong 30019, Republic of Korea

Supporting Information

ABSTRACT: A fundamental understanding of hot electron transport is critical for developing efficient hot-carrier-based solar cells. There have been significant efforts to enhance hot electron flux, and it has been found that a key factor affecting the hot electron flux is the lifetime of the hot electrons. Here, we report a combined study of hot electron flux and the lifetime of hot carriers using a perovskite-modified plasmonic nanodiode. We found that perovskite deposition on a plasmonic nanodiode can considerably improve hot electron generation induced by photon absorption. The perovskite plasmonic nanodiode consists of $MAPbI_3$ layers covering a plasmonic-Au/TiO_2 Schottky junction that is composed of randomly connected Au nanoislands deposited on a TiO_2 layer. The measured incident photon-to-electron conversion efficiency and the short-circuit photocurrent show a significantly improved solar-to-electrical conversion performance of this nanodiode. Such an improvement is ascribed to the improved hot electron flux in $MAPbI_3$ caused by effective light absorption from near-field enhancement of plasmonic Au and the efficient capture of hot electrons from Au nanoislands via the formation of a three-dimensional Schottky interface. The relation between the lifetime and flux of hot electrons was confirmed by femtosecond transient absorption spectroscopy that showed considerably longer hot electron lifetimes in $MAPbI_3$ combined with the plasmonic Au structure. These findings can provide a fundamental understanding of hot electron generation and transport in perovskite, which can provide helpful guidance to designing efficient hot carrier photovoltaics.

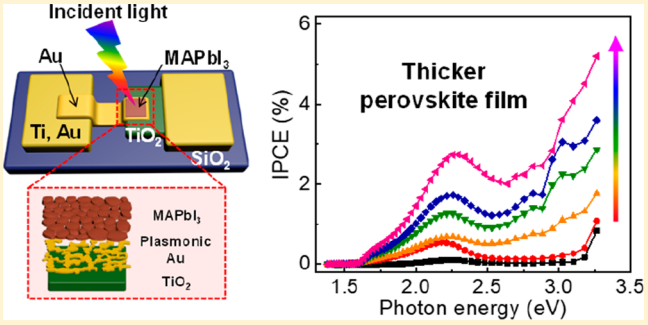

KEYWORDS: *hot electron, inorganic−organic hybrid perovskite, surface plasmon, Schottky nanodiode, hot carrier solar cells*

Photogenerated hot carriers are highly energetic with 1−3 eV of excess energy and are not in thermal equilibrium with lattice atoms.[1−5] Hot-carrier-based solar cells that utilize the generation of hot carriers have emerged as next-generation solar energy converters, as they can overcome the maximum efficiency of standard single-junction solar cells (i.e., the Shockley−Quiesser limit).[6] There have been significant efforts to enhance hot electron flux, and it has been found that the lifetime of hot electrons plays a crucial role in determining hot electron flux.[7,8]

The first scheme to utilize hot electrons for solar energy conversion was demonstrated by McFarland and Tang, who proposed a photodiode composed of dye molecules coated on a Au/TiO_2 Schottky junction.[9] The dye molecules were used as photoreceptors, by which the light harvesting process was demonstrated, but the efficiency was limited by ineffective coverage of the dye molecules, which led to low photon absorption. Using the same scheme of dyes combined with Au/TiO_2 Schottky diodes, Lee et al. generated additional localized surface plasmon resonance (LSPR) by changing the morphology of the Au thin film into connected Au islands.[10] They confirmed that the combination of dye molecules and surface plasmons exhibited a synergistic effect on the solar-to-electrical conversion efficiency because of the additional hot electron flow from the Au nanostructures and the dye molecules. Despite the ongoing active research, the efficiency of these solar cells still needs to be improved to reach practical levels. In fact, the major bottleneck for hot-electron-based photovoltaics is the rapid decay of hot electrons.[11,12] The

Received: May 16, 2019
Revised: July 23, 2019
Published: July 26, 2019

DOI: 10.1021/acs.nanolett.9b02009
Nano Lett. 2019, 19, 5489−5495

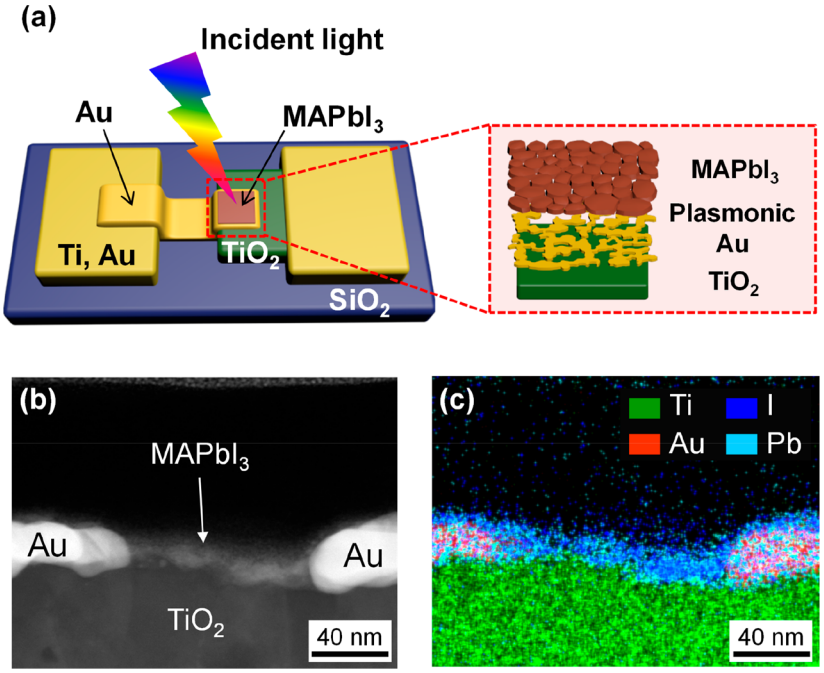

Figure 1. (a) Schematic of the $MAPbI_3$/plasmonic-Au/TiO_2 nanodiode (left) and magnified illustration of the active area (right). (b) Cross-sectional HAADF-STEM image of the $MAPbI_3$/plasmonic-Au/TiO_2 structure. (c) Cross-sectional elemental EDS mapping image of the $MAPbI_3$-covered plasmonic nanodiode.

relaxation of hot electrons occurs so quickly (i.e., less than several picoseconds[13,14]) that they lose their excess energy prior to being extracted. Therefore, a significant amount of the initial solar energy cannot be harvested, which leads to a low conversion efficiency. One suggested strategy to overcome such a critical problem is to use the LSPR effect generated in nanostructured metals.[15−18]

The LSPR effect is the resonant oscillation of free electrons in a metal nanostructure induced by an incident electromagnetic field.[1,19,20] In the case of small metal nanoparticles with small albedos, LSPR is accompanied by a strongly enhanced electric field around the metal surface, called near-field enhancement.[21−23] Such radiative effects of LSPR can concentrate incident light into the metal surface in a small volume, and the intensity of the localized electromagnetic field is several orders of magnitude higher than the incident photon flux. Near-field enhancement helps neighboring materials to effectively absorb the incident light and can also improve the generation of active carriers in the vicinity because the generation rate of electron−hole pairs is proportional to the intensity of the electric field ($|E|^2$).[22−25] On the other hand, the LSPR effect can also induce a nonradiative effect by using its energy for creating other secondary hot electrons in metal nanostructures, called Landau damping.[1,26−28] Such remarkable radiative and nonradiative effects of LSPR have motivated various efforts to develop efficient solar cells based on hot electrons.[15,16]

Recently, several researchers reported that hybrid inorganic−organic perovskites (HIOP) have outstanding hot electron properties compared with other semiconductors,[29−31] which make HIOP a promising candidate for solar cells based on hot electrons. Among them, methylammonium lead halides ($CH_3NH_3PbX_3$ (X = Cl, Br, I)), which have been actively studied for solar cell applications,[32−35] were shown to have excellent hot electron dynamics. For example, the diffusion length of hot electrons in $CH_3NH_3PbI_3$ ($MAPBI_3$) is about ∼230 nm,[31] whereas diffusion lengths of ∼20, ∼85, and ∼14 nm were observed for Si,[36] GaAs,[37] and GaN,[38] respectively. Such effective hot electron transport is attributed to slow hot carrier cooling mediated by the hot-phonon bottleneck[29] and Auger heating[39,40] effects. This effective hot electron transport can also be found in different types of HIOP because they share similar cooling dynamics.[31,41] Although such excellent hot electron properties have been found in perovskites, most studies have focused on revealing the mechanism for hot electron relaxation, and there has been little effort to utilize perovskites as hot carrier photovoltaics.

For the combined study of hot electron flux and the lifetime of hot carriers, we fabricated a $MAPbI_3$-modified plasmonic nanodiode that combines $MAPbI_3$ with the LSPR effect of nanostructured Au. $MAPbI_3$ was chosen because of its well-known photoelectrical properties and ease of fabrication. Schematic illustrations of the fabricated photonanodiode are shown in Figure 1a. The active area is composed of a solution-processed $MAPbI_3$ film stacked on a plasmonic-Au/TiO_2 Schottky nanodiode. The pure phase of the fabricated $MAPbI_3$ film was confirmed via X-ray diffraction (XRD) and its absorbance spectrum (Figure S1). Because the incident light is illuminated normal to the sample surface, the light goes sequentially through the $MAPbI_3$, the plasmonic Au, and then through the TiO_2. The active area was quantitatively investigated by cross-sectional high-angle annular dark-field (HAADF) and scanning transmission electron microscopy (STEM) images (Figure 1b) and an overlapped elemental mapping image from energy dispersive X-ray spectroscopy (EDS) (Figure 1c). The nanosized Au clusters are located on the TiO_2 layer, and the perovskite is deposited as the top layer, covering whole gold structures and filling the gaps between the Au clusters. This structure is confirmed by separate EDS elemental mapping images (Figure S2). For comparison, we also conducted experiments on the nanodiode structure with thin-film Au instead of plasmonic Au, where the LSPR effect

DOI: 10.1021/acs.nanolett.9b02009
Nano Lett. 2019, 19, 5489−5495

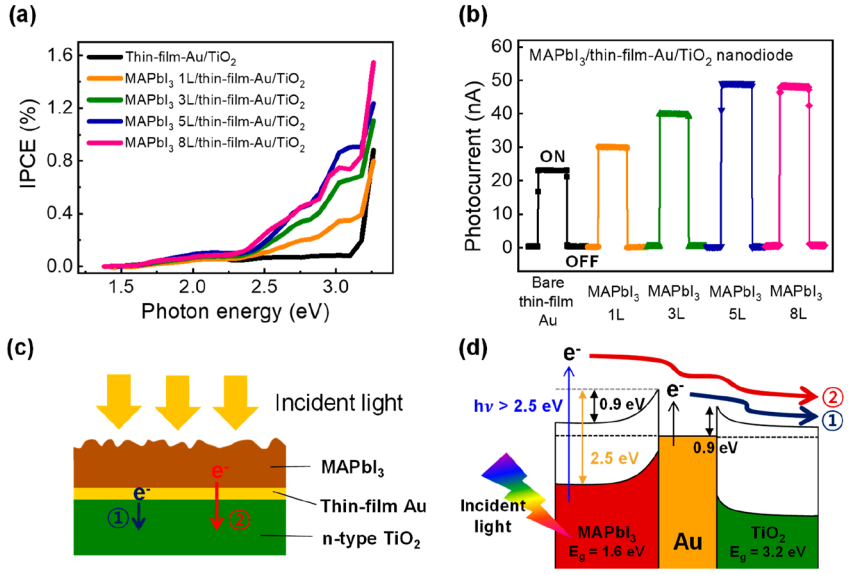

Figure 2. (a) IPCE as a function of the incident photon energy and (b) short-circuit photocurrents measured on the $MAPbI_3$/thin-film-Au/TiO_2 nanodiodes according to the number of $MAPbI_3$ layers. (c) Schematic drawing of the hot electron pathways for the $MAPbI_3$/thin-film-Au/TiO_2 structure. (d) Theoretically drawn energy levels of the $MAPbI_3$/thin-film-Au/TiO_2 structure.

does not exist. To confirm the morphology and thickness of the nanodiode, both plane and cross-sectional scanning electron microscopy (SEM) images were obtained (Figures S3 and S4). The morphology of the bare Au thin film, which is about 15 nm thick, exhibits a flat and uniform layer, while the plasmonic Au structure shows a much thicker (30 nm) and corrugated film with a portion of the area unfilled. This is because the plasmonic Au was formed by heating the Au thin film at 200 °C in ambient air. Because the Au film has a higher surface energy than the TiO_2 layer, the Au thin film undergoes morphological changes into connected Au nanoclusters at high temperature. Deposition of the perovskite film yields a densely grained layer on top of both the thin-film Au and the plasmonic Au film. In the case of plasmonic Au (Figure S4c), the nanostructured Au layer image appears brighter than the $MAPbI_3$ film because the LSPR effect of the plasmonic Au creates additional hot electrons, which can then eject more detectable electrons. Nevertheless, the $MAPbI_3$ layer is uniformly coated as the top layer fully covering the gold structures (Figure S4d).

For the experiment, we prepared plasmonic nanodiodes with several different $MAPbI_3$ thicknesses to investigate the influence of $MAPbI_3$ thickness on hot electron flow. Consideration of the mean free path of hot electrons suggests that the thickness should be several tens of nanometers; accordingly, we used perovskite precursor ink concentrations of 80 and 150 mM. The thickness of each perovskite layer is in the range of 45 to 70 nm (Figure S5). At the beginning of the experiment, the rectifying behavior of the fabricated nanodiodes was characterized by measuring the current−voltage curves (I−V curves) (Figure S6), and the Schottky barrier heights were acquired by fitting the measured I−V curves to the thermionic emission eq (Table S1). The results indicate that the nanodiodes maintain their rectifying behavior, and the change in Schottky barrier height is negligible with the perovskite modification.

To investigate the photoelectrical performance of the photonanodiodes, we measured the short-circuit photocurrent with incident light, which has a broad visible light spectrum (9 mW/cm^2), and the incident photon-to-electron conversion efficiency (IPCE) as a function of photon energy. Figure 2a, b shows the results of the IPCE and photocurrent measurements of the $MAPbI_3$-modified thin-film-Au/TiO_2 nanodiodes. In the case of the bare thin-film-Au/TiO_2, the IPCE increases slowly at first but increases rapidly in the high photon energy region (>3.2 eV). The sudden increase over 3.2 eV is ascribed to excitation from the valence band to the conduction band in the titanium oxide layer. On the other hand, deposition of the perovskite film on the thin-film-Au/TiO_2 structure results in an initial increase in the IPCE at around 2.5 eV followed by a rapid increase over 3.2 eV. To better understand hot electron transport in our diode structures, schematics of the hot electron pathways (Figure 2c) and theoretical energy levels (Figure 2d) were drawn. In terms of the energy levels, there are two Schottky barriers created on each side of the Au interface because the work function of Au is greater than that of $MAPbI_3$ and TiO_2. The built-in potential in the $MAPbI_3$ (~0.9 eV) and the Schottky barrier at the Au/TiO_2 interface (~0.9 eV) play roles as energy barriers so that only highly energetic carriers (hot electrons) can be collected. According to theoretical energy levels, a minimum photon energy of 2.5 eV is necessary to collect hot electrons from the perovskite film, and thus, the initial increase around 2.5 eV can originate from hot electrons excited in the $MAPbI_3$. This hypothesis is further supported by the prominent increase around 2.5 eV with the thicker perovskite film, which is caused by the thicker perovskite film absorbing more incident photons to generate more hot electrons. Correspondingly, the short-circuit photocurrent of the bare thin-film-Au/TiO_2 is 25 nA but that of the $MAPbI_3$-modified thin-film-Au/TiO_2 nanodiodes increased from 30 to 50 nA as a thicker perovskite layer was deposited. However, when the thickness of the perovskite film increased further to 70 nm, the photocurrent decreased to 30 nA (Figure S7a). This is because the hot electrons are scattered in the perovskite film within their mean free path, which supports that the measured photocurrent is dominated by hot electron flow. Therefore, the enhancement of photocurrent with the deposition of a perovskite film is attributed to additional hot

DOI: 10.1021/acs.nanolett.9b02009
Nano Lett. 2019, 19, 5489−5495

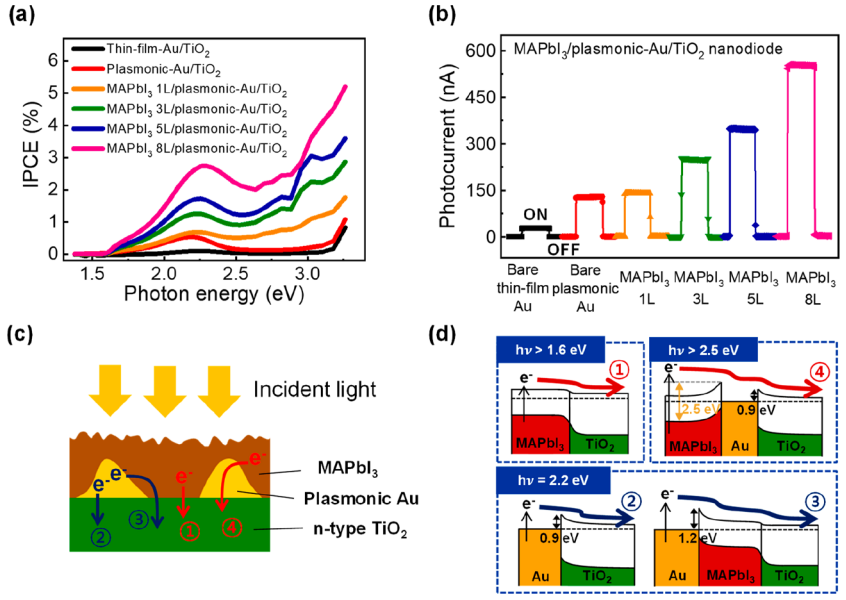

Figure 3. (a) IPCE as a function of incident photon energy and (b) short-circuit photocurrents measured on the $MAPbI_3$/plasmonic-Au/TiO_2 nanodiodes according to the number of $MAPbI_3$ layers. (c) Schematic drawing of the hot electron pathways for the $MAPbI_3$/plasmonic-Au/TiO_2 structure. (d) Theoretically drawn energy levels of the $MAPbI_3$/plasmonic-Au/TiO_2 structure.

electron flow from the $MAPbI_3$ film (pathway 2) as well as hot electron flow from the Au thin layer (pathway 1).

On the other hand, for the $MAPbI_3$/plasmonic-Au/TiO_2 nanodiodes, the IPCE peaks show a marked increase in three different photon energy regions (Figure 3a), and they also demonstrate highly improved photocurrents (Figure 3b). The hot electron pathways and theoretical energy levels in this structure are illustrated in Figure 3c, d. The first IPCE peak at 1.6 eV is from excited electrons extracted at the conduction band edge of the $MAPbI_3$ resulting from the inevitable formation of a direct p−n junction between the $MAPbI_3$ and the TiO_2 in the plasmonic Au nanodiode (pathway 1). The second IPCE peak occurs at 2.2 eV, which is dominated by hot electron flow generated from the plasmonic Au layer. In other words, when the morphology of the bare thin-film Au changes into plasmonic Au, the diode shows a strong IPCE enhancement at 2.2 eV. This is because the LSPR effect occurs strongly in that particular photon energy region and creates additional secondary hot electrons contributing to increase the IPCE. Interestingly, the second IPCE peaks show further improvement with perovskite film deposition compared with the bare plasmonic-Au/TiO_2 nanodiode. Because contact between the $MAPbI_3$ and Au also creates a Schottky junction, hot electrons in the plasmonic Au can be collected not only through the bottom Schottky interface (pathway 2) but also via the lateral Schottky interface (pathway 3). It is well-known that the formation of three-dimensional Schottky junctions can considerably enhance the short-circuit photocurrent because of the increased extraction possibility for hot electrons with both transverse and longitudinal momenta.[42−44] Lastly, the third IPCE enhancement is observed over 2.5 eV, which is attributed to hot electron extraction from the $MAPbI_3$ film. The measured photocurrent (Figure 3b) is 25 nA on the bare thin-film-Au/TiO_2, which increases to 128 nA after changing the surface morphology to plasmonic Au. Perovskite film modification leads to further photocurrent enhancement from 139 to 552 nA. These results indicate that hot electrons created in the plasmonic Au can be efficiently extracted by the formation of a three-dimensional Schottky interface, and additional hot electron flow from the perovskite film can significantly enhance the photoconversion performance compared with bare thin-film Au and plasmonic Au counterparts. However, the photocurrent decreased dramatically to 120 nA (Figure S7b) when the perovskite film thickness reached 70 nm because of hot electron scattering within the electron mean free path.

To give detailed insight into the LSPR effect on hot electron flow, we compared the results from the $MAPbI_3$/thin-film-Au/TiO_2 nanodiodes and their $MAPbI_3$/plasmonic-Au/TiO_2 counterparts where identical perovskite layers were used (Figure S8). The $MAPbI_3$ coupled with LSPR structures show higher IPCEs in most of the photon energy region, and the short-circuit photocurrents were increased by factors of 5, 6, 7, and 12 for the single-, 3-, 5-, and 8-layered $MAPbI_3$, respectively. To reveal the effect of $MAPbI_3$ combined with LSPR, the absorbance spectrum was obtained from $MAPbI_3$ coated on thin-film Au and on plasmonic Au structures (Figure S9). In the low photon energy region (<2.7 eV), a strong absorbance peak is observed for the $MAPbI_3$/plasmonic-Au structure (Figure S9a), which is in the identical region as the LSPR absorbance peak (Figure S9b). Thus, IPCE enhancement below 2.7 eV can be ascribed to an increased number of Au hot electrons assisted by the LSPR effect. On the other hand, there is a negligible difference in the absorbance in the high photon energy region (>2.7 eV), but the IPCE is considerably higher for the $MAPbI_3$/plasmonic-Au/TiO_2. We suggest that this higher IPCE can be attributed to near-field enhancement generated by LSPR in the Au nanostructure, which causes the incident light to be focused on the plasmonic Au surface with greater intensity. Thus, the $MAPbI_3$, which is located near the plasmonic Au, can efficiently absorb light, which increases hot electron−hole pair generation. This can also be verified by the higher photoluminescence intensity of the $MAPbI_3$ with an LSPR structure (Figure S10), where more hot electrons can give a higher emission intensity. Furthermore, the hot electrons are generated near the hot

DOI: 10.1021/acs.nanolett.9b02009
Nano Lett. 2019, 19, 5489−5495

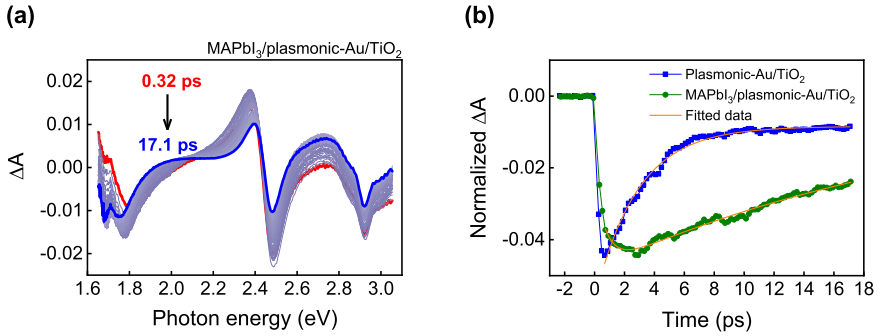

Figure 4. (a) Transient absorption spectra of the $MAPbI_3$/plasmonic-Au/TiO_2 structure with photoexcitation at 3.0 eV. (b) Time profile of the normalized time-resolved absorption changes probed at 1.8 eV for the plasmonic-Au/TiO_2 and the $MAPbI_3$/plasmonic-Au/TiO_2 structure after photoexcitation at 3.0 eV.

spot of the plasmonic Au structure; thus, efficient hot electron extraction can be driven on the perovskite-deposited plasmonic Au structure compared with the $MAPbI_3$/thin-film-Au structure. Therefore, $MAPbI_3$ coupled with the LSPR effect can give IPCE and short-circuit photocurrent values higher than $MAPbI_3$ without the LSPR effect.

In addition to the enhanced photoconversion performance of the perovskite-modified plasmonic Au structure, we carried out femtosecond transient absorption (TA) experiments to elucidate the ultrafast hot electron relaxation dynamics. Because the samples must absorb sufficient light for the TA experiment, we modified the sample preparation to make thicker layers. The detailed sample preparation procedures and characterization are provided in the Methods section and in Figure S11 in the Supporting Information. The TA spectra of the $MAPbI_3$/plasmonic-Au/TiO_2 structure were obtained with photoexcitation at 3.0 eV (Figure 4a). The TA spectra of the TiO_2 film deposited on quartz were measured in advance to ensure that the TiO_2 and substrate were not influenced by the pump beam. Indeed, the TiO_2 film deposited on quartz did not exhibit any signal across the entire range of the probe photon energy after excitation at 3.0 eV (Figure S12). In addition to the $MAPbI_3$/plasmonic-Au/TiO_2 structure, the TA spectra of the thin-film-Au/TiO_2 and plasmonic-Au/TiO_2 were also obtained (Figure S13) for comparison. According to the acquired TA spectra, the thin-film-Au/TiO_2 exhibits only a positive band centered at 2.4 eV, while the plasmonic-Au/TiO_2 shows both a positive band at 2.4 eV and a negative band at 1.8 eV. It is known that gold nanoparticles with a diameter of less than 10 nm have a positive absorption band at 2.6 eV, which is related to interband excitation in the gold nanostructures, and a negative bleaching band at 2.3 eV, which is associated with depletion of surface plasmon electrons.[45,46] The larger size of our plasmonic-Au structure lead to a red-shifted plasmon band; therefore, the negative bleaching band at 1.8 eV for the plasmonic-Au/TiO_2 is created by the LSPR effect. In the case of the $MAPbI_3$/plasmonic-Au/TiO_2, several earlier reports revealed that the high photon energy tail (ranging from 1.7 to 1.8 eV) of $MAPbI_3$ ground state bleaching is attributed to hot-carrier distribution.[29,47,48] The time-resolved decay profiles of the plasmonic-Au/TiO_2 and $MAPbI_3$/plasmonic-Au/TiO_2 structures probed at 1.8 eV are plotted in Figure 4b to better understand the cooling dynamics of hot electrons from plasmonic Au and $MAPbI_3$. The whole decay profile of the $MAPbI_3$/plasmonic-Au/TiO_2 structure probed with longer delay times is shown in Figure S14. The time components are measured by fitting the decay profiles into a single exponential function ($A\exp(-t/\tau_1)$) for the plasmonic-Au/TiO_2 and a biexponential function ($A_1\exp(-t/\tau_1) + A_2\exp(-t/\tau_2)$) for the $MAPbI_3$/plasmonic-Au/TiO_2; the fitted results are summarized in Table 1. The acquired time components of the

Table 1. Summary of the Fit Parameters for the Plasmonic-Au/TiO_2 and $MAPbI_3$/Plasmonic-Au/TiO_2 Structure

sample	$h\nu_{probe}$ (eV)	time constants (ps) τ_1	τ_2
plasmonic-Au/TiO_2	1.8	2.87 ± 0.06	
$MAPbI_3$/plasmonic-Au/TiO_2	1.8	0.75 ± 0.10	62.38 ± 1.13

plasmonic-Au/TiO_2 structures show a time constant of 2.87 ps, which is commensurate with the electron−phonon scattering lifetime of hot electrons in gold nanoparticles.[45,49−51] Meanwhile, the $MAPbI_3$/plasmonic-Au/TiO_2 structure describes two time constants (0.75 and 62.38 ps). We suggest that the long time constant (62.38 ps) originated from the $MAPbI_3$ hot electron lifetime within the conduction band because the hot electron lifetime for perovskite bulk film is known to be ∼100 ps.[29,31,48] Because hot electron relaxation times are determined by hot-carrier densities and the crystallinity of the film, the shorter lifetime in our system can be explained by unfavorable light absorption because of the thin film (∼80 nm) and small grain sizes (less than 100 nm). The fast time constant (0.75 ps) of the $MAPbI_3$/plasmonic-Au/TiO_2 is ascribed to a hot electron trap at the grain boundaries. We associate this with the PbI_2 bleaching peak at 2.5 eV in the $MAPbI_3$/plasmonic-Au/TiO_2 TA spectra, which means that some portion of the grain boundaries are unfilled and become trap states.[52] Although the probe photon energy of 1.8 eV is governed by hot electron decay from both the plasmonic Au and the $MAPbI_3$, we cannot obtain the plasmonic Au hot electron lifetime (2.87 ps) and can acquire only the $MAPbI_3$ hot electron lifetimes (0.75 and 62.38 ps) from the $MAPbI_3$/plasmonic-Au/TiO_2 structure. This is because the $MAPbI_3$ layer absorbs the majority of the photons before the plasmonic Au; thus, the $MAPbI_3$ hot electrons become dominant. According to the fit parameters, there are obvious features showing that the $MAPbI_3$ hot electrons exhibit inherently long lifetimes, which are ∼22 times longer than that of Au hot electrons. We expect that the $MAPbI_3$/thin-film-Au/TiO_2 structure exhibits a much shorter hot electron lifetime, compared with the $MAPbI_3$/plasmonic-Au/TiO_2 structure because of rapid hot electron relaxation. In case of the metal

DOI: 10.1021/acs.nanolett.9b02009
Nano Lett. 2019, 19, 5489−5495

planar film, we can assume that electrons are mainly scattered at the interface with few being transmitted. The scattering of hot electrons can be induced at the metal−semiconductor interface because of the high potential step and large electron effective mass mismatch at the interface;[53,54] thus, the hot electrons are likely to dissipate into phonon modes and surrounding carriers, giving rise to the short hot carrier lifetime.

In addition, we can at least suggest that the combination of $MAPbI_3$ and the plasmonic Au structure shows a significantly increased hot electron lifetime compared with the plasmonic-Au/TiO_2 structure because of the slow hot electron cooling time of the perovskite, which can contribute to the higher photoelectrical conversion efficiency. We anticipate that these findings can also be applied to other types of HIOPs with comparable hot electron properties as $MAPbI_3$, and these results can provide a fundamental understanding of hot electron generation and transport in perovskite. Further work for designing efficient photovoltaics based on perovskite hot electrons can be done by tuning the time scales of hot electron thermalization and extraction to realize a sufficient thermal hot electron population. Alternatively, adopting a tandem or tunneling structure with the suggested cell, which utilizes a broad spectrum of wavelengths, can be a helpful approach as well.

In summary, we fabricated $MAPbI_3$-modified plasmonic-Au/TiO_2 nanodiodes and observed enhanced hot electron generation from the LSPR effect of the Au nanostructure measured using IPCE and the short-circuit photocurrent. We confirmed that $MAPbI_3$ deposition on both thin-film Au and plasmonic Au structures leads to increased photocurrent by creating additional hot electron flow from the $MAPbI_3$ as well as from the Au layer. $MAPbI_3$ deposited on a plasmonic-Au/TiO_2 nanodiode showed even greater enhancement because the formation of a three-dimensional Schottky interface promotes effective hot electron extraction in the plasmonic Au, and the generation of $MAPbI_3$ hot electrons is enhanced because of the near-field enhancement. Furthermore, using femtosecond transient absorption experiments, we observed significantly prolonged hot electron lifetimes in $MAPbI_3$ coupled with a LSPR structure, which can be related to the very high photocurrent in the $MAPbI_3$/plasmonic-Au/TiO_2 nanodiode. These results have meaningful applications in that we revealed the synergistic interaction between $MAPbI_3$ and surface plasmons of gold by showing hot electron transport mechanisms with systematic structure variation at the interface using a macroscale photonanodiode. We reveal the origin of each hot electron flow that contributes to the overall photocurrent using photon energy dependence experiments and theoretical energy levels. The majority of hot electron studies for perovskites has focused on hot carrier relaxation dynamics, and thus, the variation of hot electron transport depending on changes in the interfacial structure was not well-understood.

■ ASSOCIATED CONTENT

Supporting Information

The Supporting Information is available free of charge on the ACS Publications website at DOI: 10.1021/acs.nanolett.9b02009.

Detailed sample preparation procedure, XRD results, absorbance spectra, EDS elemental mapping images, SEM images, $I-V$ curves, and TA spectra of samples (PDF)

■ AUTHOR INFORMATION

Corresponding Authors

*E-mail: hyotcherl.ihee@kaist.ac.kr.
*E-mail: jeongypark@kaist.ac.kr.

ORCID

Dae Won Cho: 0000-0002-4785-069X
Nam-Gyu Park: 0000-0003-2368-6300
Hyotcherl Ihee: 0000-0003-0397-5965
Jeong Young Park: 0000-0002-8132-3076

Notes

The authors declare no competing financial interest.

■ ACKNOWLEDGMENTS

This work was supported by the Institute for Basic Science (IBS-R004). N.G.P. acknowledges support from National Research Foundation of Korea (NRF) grants funded by the Ministry of Science, ICT Future Planning (MSIP) of Korea under Contracts NRF-2012M3A6A7054861 and NRF-2014M3A6A7060583 (Global Frontier R&D Program on Center for Multiscale Energy System). We thank Doo-Sik Ahn for the helpful discussion.

■ REFERENCES

(1) Brongersma, M. L.; Halas, N. J.; Nordlander, P. *Nat. Nanotechnol.* **2015**, *10*, 25−34.
(2) Nienhaus, H. *Surf. Sci. Rep.* **2002**, *45*, 1−78.
(3) Somorjai, G. A.; Frei, H.; Park, J. Y. *J. Am. Chem. Soc.* **2009**, *131*, 16589−16605.
(4) Park, J. Y.; Baker, L. R.; Somorjai, G. A. *Chem. Rev.* **2015**, *115*, 2781−2817.
(5) Lee, Y. K.; Lee, H.; Park, J. Y. *Sci. Rep.* **2015**, *4*, 4580.
(6) Ross, R. T.; Nozik, A. J. *J. Appl. Phys.* **1982**, *53*, 3813−3818.
(7) Conibeer, G. J.; Konig, D.; Green, M. A.; Guillemoles, J. F. *Thin Solid Films* **2008**, *516*, 6948−6953.
(8) Pandey, A.; Guyot-Sionnest, P. *Science* **2008**, *322*, 929−932.
(9) McFarland, E. W.; Tang, J. *Nature* **2003**, *421*, 616−618.
(10) Lee, Y. K.; Park, J.; Park, J. Y. *J. Phys. Chem. C* **2012**, *116*, 18591−18596.
(11) Nozik, A. J. *Nat. Energy* **2018**, *3*, 170−171.
(12) Fang, H. H.; Adjokatse, S.; Shao, S. Y.; Even, J.; Loi, M. A. *Nat. Commun.* **2018**, *9*, 243.
(13) Hodak, J. H.; Martini, I.; Hartland, G. V. *J. Phys. Chem. B* **1998**, *102*, 6958−6967.
(14) Nozik, A. J. *Annu. Rev. Phys. Chem.* **2001**, *52*, 193−231.
(15) Lee, H.; Lee, Y. K.; Hwang, E.; Park, J. Y. *J. Phys. Chem. C* **2014**, *118*, 5650−5656.
(16) Lee, Y. K.; Jung, C. H.; Park, J.; Seo, H.; Somorjai, G. A.; Park, J. Y. *Nano Lett.* **2011**, *11*, 4251−4255.
(17) Liu, X.; Cuenya, B. R.; McFarland, E. W. *Sens. Actuators, B* **2004**, *99*, 556−561.
(18) Wang, F. M.; Melosh, N. A. *Nano Lett.* **2011**, *11*, 5426−5430.
(19) Atwater, H. A.; Polman, A. *Nat. Mater.* **2010**, *9*, 205−213.
(20) Clavero, C. *Nat. Photonics* **2014**, *8*, 95−103.
(21) Erwin, W. R.; Zarick, H. F.; Talbert, E. M.; Bardhan, R. *Energy Environ. Sci.* **2016**, *9*, 1577−1601.
(22) Valenti, M.; Jonsson, M. P.; Biskos, G.; Schmidt-Ott, A.; Smith, W. A. *J. Mater. Chem. A* **2016**, *4*, 17891−17912.
(23) Linic, S.; Christopher, P.; Ingram, D. B. *Nat. Mater.* **2011**, *10*, 911−921.
(24) Anger, P.; Bharadwaj, P.; Novotny, L. *Phys. Rev. Lett.* **2006**, *96*, 113002.

DOI: 10.1021/acs.nanolett.9b02009
Nano Lett. 2019, 19, 5489−5495

(25) Lee, J.; Javed, T.; Skeini, T.; Govorov, A. O.; Bryant, G. W.; Kotov, N. A. *Angew. Chem., Int. Ed.* **2006**, *45*, 4819−4823.
(26) Li, W.; Valentine, J. G. *Nanophotonics* **2017**, *6*, 177−191.
(27) Lee, Y. K.; Lee, H.; Lee, C.; Hwang, E.; Park, J. Y. *J. Phys.: Condens. Matter* **2016**, *28*, 254006.
(28) Li, X. G.; Xiao, D.; Zhang, Z. Y. *New J. Phys.* **2013**, *15*, 023011.
(29) Yang, Y.; Ostrowski, D. P.; France, R. M.; Zhu, K.; van de Lagemaat, J.; Luther, J. M.; Beard, M. C. *Nat. Photonics* **2016**, *10*, 53−59.
(30) Zhu, H. M.; Miyata, K.; Fu, Y. P.; Wang, J.; Joshi, P. P.; Niesner, D.; Williams, K. W.; Jin, S.; Zhu, X. Y. *Science* **2016**, *353*, 1409−1413.
(31) Guo, Z.; Wan, Y.; Yang, M. J.; Snaider, J.; Zhu, K.; Huang, L. B. *Science* **2017**, *356*, 59−62.
(32) Kim, H. S.; Lee, C. R.; Im, J. H.; Lee, K. B.; Moehl, T.; Marchioro, A.; Moon, S. J.; Humphry-Baker, R.; Yum, J. H.; Moser, J. E.; Gratzel, M.; Park, N. G. *Sci. Rep.* **2012**, *2*, 591.
(33) Im, J. H.; Jang, I. H.; Pellet, N.; Gratzel, M.; Park, N. G. *Nat. Nanotechnol.* **2014**, *9*, 927−932.
(34) Ono, L. K.; Wang, S. H.; Kato, Y.; Raga, S. R.; Qi, Y. B. *Energy Environ. Sci.* **2014**, *7*, 3989−3993.
(35) Ono, L. K.; Juarez-Perez, E. J.; Qi, Y. B. *ACS Appl. Mater. Interfaces* **2017**, *9*, 30197−30246.
(36) Bernardi, M.; Vigil-Fowler, D.; Lischner, J.; Neaton, J. B.; Louie, S. G. *Phys. Rev. Lett.* **2014**, *112*, 257402.
(37) Hayes, J. R.; Levi, A. F. J. *IEEE J. Quantum Electron.* **1986**, *22*, 1744−1752.
(38) Suntrup, D. J.; Gupta, G.; Li, H. R.; Keller, S.; Mishra, U. K. *Appl. Phys. Lett.* **2014**, *105*, 263506.
(39) Fu, J. H.; Xu, Q.; Han, G. F.; Wu, B.; Huan, C. H. A.; Leek, M. L.; Sum, T. C. *Nat. Commun.* **2017**, *8*, 1300.
(40) Li, M. J.; Bhaumik, S.; Goh, T. W.; Kumar, M. S.; Yantara, N.; Gratzel, M.; Mhaisalkar, S.; Mathews, N.; Sum, T. C. *Nat. Commun.* **2017**, *8*, 14350.
(41) Madjet, M. E. A.; Akimov, A. V.; El-Mellouhi, F.; Berdiyorov, G. R.; Ashhab, S.; Tabet, N.; Kais, S. *Phys. Chem. Chem. Phys.* **2016**, *18*, 5219−5231.
(42) Lee, C.; Choi, H.; Nedrygailov, I. I.; Lee, Y. K.; Jeong, S.; Park, J. Y. *ACS Appl. Mater. Interfaces* **2018**, *10*, 5081−5089.
(43) Lee, C.; Lee, Y. K.; Park, Y.; Park, J. Y. *ACS Photonics* **2018**, *5*, 3499−3506.
(44) Knight, M. W.; Wang, Y. M.; Urban, A. S.; Sobhani, A.; Zheng, B. Y.; Nordlander, P.; Halas, N. J. *Nano Lett.* **2013**, *13*, 1687−1692.
(45) Karam, T. E.; Khoury, R. A.; Haber, L. H. *J. Chem. Phys.* **2016**, *144*, 124704.
(46) Logunov, S. L.; Ahmadi, T. S.; ElSayed, M. A.; Khoury, J. T.; Whetten, R. L. *J. Phys. Chem. B* **1997**, *101*, 3713−3719.
(47) Price, M. B.; Butkus, J.; Jellicoe, T. C.; Sadhanala, A.; Briane, A.; Halpert, J. E.; Broch, K.; Hodgkiss, J. M.; Friend, R. H.; Deschler, F. *Nat. Commun.* **2015**, *6*, 8420.
(48) Li, M. J.; Bhaumik, S.; Goh, T. W.; Kumar, M. S.; Yantara, N.; Gratzel, M.; Mhaisalkar, S.; Mathews, N.; Sum, T. C. *Nat. Commun.* **2017**, *8*, 14350.
(49) Furube, A.; Du, L.; Hara, K.; Katoh, R.; Tachiya, M. *J. Am. Chem. Soc.* **2007**, *129*, 14852−14853.
(50) Link, S.; El-Sayed, M. A. *Int. Rev. Phys. Chem.* **2000**, *19*, 409−453.
(51) Link, S.; El-Sayed, M. A. *J. Phys. Chem. B* **1999**, *103*, 8410−8426.
(52) Wang, L. L.; McCleese, C.; Kovalsky, A.; Zhao, Y. X.; Burda, C. *J. Am. Chem. Soc.* **2014**, *136*, 12205−12208.
(53) Smith, D. L.; Lee, E. Y.; Narayanamurti, V. *Phys. Rev. Lett.* **1998**, *80*, 2433−2436.
(54) Kozhevnikov, M.; Narayanamurti, V.; Zheng, C.; Chiu, Y. J.; Smith, D. L. *Phys. Rev. Lett.* **1999**, *82*, 3677−3680.

DOI: 10.1021/acs.nanolett.9b02009
Nano Lett. 2019, 19, 5489−5495